JOURNAL OF AEROSOL MEDICINE AND PULMONARY DRUG DELIVERY
Volume 28, Number 2, 2015

Pp. 116–129
DOI: 10.1089/jamp.2013.1120

Analysis of Three-Dimensional Aerosol Deposition in Pharmacologically Relevant Terms: Beyond Black or White ROIs

Elliot Eliyahu Greenblatt, MS,[1,2] Tilo Winkler, PhD,[2] Robert Scott Harris, MD,[3] Vanessa Jane Kelly, PhD,[3] Mamary Kone, MD,[3] and Jose Venegas, PhD[2]

Abstract

Background: This article presents a novel methodological approach to evaluate images of aerosol deposition taken with PET-CT cameras. Traditionally, Black-or-White (BW) Regions of Interest (ROIs) are created to cover Anatomical Regions (ARs) segmented from the high-resolution CT. Such ROIs do not usually consider blurring effects due to limited spatial resolution or breathing motion, and do not consider uncertainty in the AR position within the PET image. The new methodology presented here (Grayscale) addresses these issues, allows estimates of aerosol deposition within ARs, and expresses the deposition in terms of Tissue Dosing (in the lung periphery) and Inner Surface Concentration (in the larger airways).

Methods: Imaging data included a PET deposition image acquired during breathing and two CT scans acquired during breath holds at different lung volumes. The lungs were segmented into anatomically consistent ARs to allow unbiased comparisons across subjects and across lobes. The Grayscale method involves defining Voxel Influence Matrices (VIMs) to consider how average activity within each AR influences the measured activity within each voxel. The BW and Grayscale methods were used to analyze aerosol deposition in 14 bronchoconstricted asthmatics.

Results: Grayscale resulted in a closer description of the PET image than BW ($p<0.0001$) and exposed a seven-fold underestimation in measures of specific deposition. The Average Tissue Dosing was 2.11×10^{-6} Total Lung Dose/mg. The average Inner Surface Concentration was 45×10^{-6} Total Lung Dose/mm^2, with the left lower lobe having a lower ISC than lobes of the right lung ($p<0.05$). There was a strong lobar heterogeneity in these measures (COV=0.3).

Conclusion: The Grayscale approach is an improvement over the BW approach and provides a closer description of the PET image. It can be used to characterize heterogeneous concentrations throughout the lung and may be important in translational research and in the evaluation of aerosol delivery systems.

Key words: heterogeneity, motion correction, mucocilliary transport, partial volume effect, PET-CT, ROIs, spillover effect, surface concentration, tissue dosing

Introduction

Estimation of local dosing in terms of the pharmacologically relevant parameters is necessary to bridge *in vitro* and animal model experiments to the human scale. Additionally, evaluation of local dose is important to understand the regional and global effectiveness of an inhaled drug. Accurate assessment of aerosol deposition along the airway tree and the concentration of deposition on the airway surface are also useful to evaluate airway functional features, such as mucocilliary clearance rate, and to test *in vivo* the validity of computational models of aerosol delivery. The deposition of radioactive aerosol particles in the lung can be assessed in three dimensions (3D) with limited spatial resolutions using Positron Emission Tomography (PET)[1,2] and Single Photon Emission Computed Tomography (SPECT).[3] Co-registered High Resolution Computed Tomography (HRCT) images, obtained from PET-CT and SPECT-CT

[1]Department of Mechanical Engineering, Massachusetts Institute of Technology, Cambridge, MA, 02142.
Departments of [2]Anesthesia and [3]Critical Care Medicine, Massachusetts General Hospital and Harvard Medical School, Boston, MA, 02114.

instruments, provide anatomical detail that could be used to localize the observed radioactivity within specific Anatomical Regions (ARs) and thus, to evaluate regional dosing of inhaled pharmacological agents.

The standard approach to evaluate local concentration of a radiolabeled substance is to measure the average activity per unit volume within defined Regions of Interest (ROIs). ROIs are binary black or white (BW) masks that serve to group voxels corresponding to specific ARs. These ROIs are either defined based on generalizations of the anatomy,[1,2,4,5] or are segmented from detailed HRCT scans,[3,6] when available. In the lungs, it is helpful to segment the lungs into ARs that encompass a portion of the central airway tree and the lung periphery. However, the number, size, and location of airways that can be accurately segmented from HRCT images can vary substantially among subjects and within lobes, and may depend (among other factors) on the lung volume at which the CT images are acquired. Therefore a method to segment the lungs into *consistent* ARs is required to compare aerosol deposition across subjects and among lobes.

Even after defining consistent ARs, other challenges need to be confronted before aerosol deposition can be accurately evaluated; regional deposition quantification with BW ROIs may be inaccurate due to partial volume and spill-over effects.[7–9] These inaccuracies are caused by image blurring due to the limited spatial resolution of the nuclear imaging methods ($\sim$6 and $\sim$15 mm, for PET and SPECT, respectively) and by the breathing motion of the lung during imaging. Also, although PET (or SPECT) images are automatically co-registered with the CT images in combined imaging instruments (i.e., PET-CT or SPECT-CT), shifts in patient position, or differences in average lung volume between the PET and CT images, often require additional co-registration. The co-registration process includes errors that need to be considered when estimating regional activity.

Here we present a method to evaluate aerosol deposition that accounts for the effects described above by expanding the concept of BW ROIs into the Grayscale domain. To accomplish this, a Voxel Influence Matrix (VIM) is defined to describe how activity originating from an AR is sampled in each image voxel. VIMs include the combined effect of sources of blurring such as breathing motion, limited spatial resolution, registration, and model uncertainties, and allows quantification of activity from airways within ARs with dimensions smaller than the spatial resolution of the nuclear medicine method.

Applied together, these methods leverage the high anatomical detail provided by HRCT to *consistently* estimate the distribution of aerosol among specified ARs, to more *accurately* describe the deposition image, and to describe such a distribution in pharmacologically relevant terms such as airway inner surface concentration (ISC), and peripheral tissue dosing (TD). These new concepts and algorithms were implemented and used to analyze the heterogeneity of ISC and TD at a lobar level within the lungs of bronchoconstricted asthmatic subjects.

Methods

The methods are separated into sections that describe portions of the process required to leverage information within the HRCTs to interpret PET deposition images.

Imaging material and methods

This section describes the methods of acquiring the PET and CT images. The protocol was approved by the Massachusetts General Hospital Internal Review Board (Application No. 2007P000493).

Image acquisition. Fourteen mild-to-moderate asthmatic subjects were imaged the supine position with a PET-CT (Biograph 64; Siemens AG). The subjects were young (average 20.1 years), and predominantly female (4 male and 10 female) with BMI's less than 32. All subjects were mild intermittent or mild persistent asthmatics as defined by the NIH Global Initiative for Asthma[10] with FEV_1 and FVC $\geq$80% predicted, less than daily symptoms, and peak flow or FEV_1 variability of less than 30%. All subjects demonstrated reversible obstruction ($\geq$12% on previous PFT's).

Bronchoconstriction was induced with five deep breaths of aerosolized methacholine via a DeVilbiss nebulizer and Rosenthal dosimeter (model 646, DeVilbiss Healthcare, Somerset, PA) while in the scanner. Methacholine concentration was equal to the subject's previously-determined PC_{20} (the dose causing a 20% reduction in FEV_1). Two HRCT images were obtained during breath hold: one at total lung capacity before bronchoconstriction (TLC), and a second at mean lung volume after constriction (MLV). MLV was estimated as the average lung volume during quiet breathing in a 30 sec window prior to image collection. A signal proportional to instantaneous lung volume was acquired with an inductance plethysmograph (SomnoStar PT, SensorMedics Corp, Yorba Linda, CA). A trace of the instantaneous volume signal was presented to the subject on video goggles who, following a breath to TLC, was instructed to stop breathing and hold his/her breath when the trace reached a line defining his/her MLV.

An aerosol of ^{13}N-NH3 labeled isotonic saline was generated with a vibrating mesh nebulizer (Aeroneb Solo, Aerogen, Galway, Ireland) and delivered via an Idehaler holding chamber (Aerodrug, Cedex, France) into a mouthpiece. The aerosol reaching the mouthpiece was previously characterized by laser diffraction as having a 4.9 μm VMD with a GSD of 1.8.[11] Intrapulmonary aerosol deposition was imaged with dynamic PET during a period of 2 min inhalation, and the next 8 min, while they lay supine in the PET-CT camera gantry. During the study the subjects wore a mouthpiece and a nose clip, and were allowed to breath freely at their chosen tidal volume, breathing frequency, and average lung volume.

CT settings. Full chest HRCT scans were acquired in the supine position during a short breath hold ($\sim$12 sec) at the specified lung volumes (MLV and TLC). The scanner was used in a helical mode to acquire 64 slices per rotation with 0.6 mm collimation, and a pitch of 1 mm. The energy settings were 120 kV peak, and 80 mA. Image reconstruction was done using the B31F kernel with a 0.75 mm slice thickness (0.5 mm slice increment and 0.25 mm overlap). The kernel was recommended by the developers of the Apollo segmentation software used to identify the Anatomical Regions (ARs). Each HRCT results in approximately 3.2 mSv of radiation exposure. Reconstruction of the image with a reduced field of view resulted in typical voxel dimensions of $0.6 \times 0.6 \times 0.5$ mm.

PET settings. The PET images were acquired in list mode and reconstructed using filtered back projection. Attenuation correction was performed using the CT image acquired at MLV. The subject was positioned on the scanner such that the PET imaging field covered 16 cm above the dome of the diaphragm. The PET imaging field covered $83 \pm 8\%$ of the lung volume, with $4 \pm 3\%$ missing from the apex, and $13 \pm 7\%$ missing from the base. A deposition image was constructed by averaging the regional activity acquired for 7.5 min, starting 30 sec after the end of the aerosol inhalation. The NH_3 PET image results in less than 1 mSv of radiation exposure, and typical reconstruction voxels are $5 \times 5 \times 2$ mm.

Segmentation methods

To identify consistent ARs from the HRCT images the following methods were used.

Lobe and airway segmentation. For each of the two HRCT scans, the lobes and the central airway tree were segmented and airways (up to the sub-segmental airways) were labeled automatically using Apollo™ software (Vida Diagnostics, Mountain View, CA). The segmentations and airway labeling were visually validated and manually corrected when required. The location of airway bifurcations and the airway dimensions were extracted from the software output.

Isolating a consistent portion of the airway tree. The number of airway generations that could be segmented within a lobe varied between subjects and between lobes. In order to avoid bias in analysis across subjects and among regions of the lung, it was important to define a set of airways that could be quantified systematically in all lobes in every subject and in every lobe. Though all sub-segmental airways were visible at TLC in all subjects, it was not always possible to identify with certainty their distal bifurcation (the feature needed for defining the end of an airway). Therefore sub-segmental airways were trimmed to a length equal to a fixed fraction of the average length of the segmental airways of that subject. This fraction (0.74) was calculated by averaging the daughter-to-parent length ratios between generations 3–4, 4–5, and 5–6 taken from a symmetric model,[12] which correspond to the generations of sub-segmental to segmental airways in different lobes (Fig. 1A).

Defining airway and peripheral ARs. To define airway ARs, the trimmed airway trees were segmented into nine ARs. Of these, five lobar portions were defined as all airways distal to and including the corresponding lobar bronchi: left upper lobe (LUL), left lower lobe (LLL), right upper lobe (RUL), right middle lobe (RML), and right lower lobe (RLL). The remaining airway tree was segmented into four additional ARs: the intermediate bronchus (BINT), the right main bronchus (RMB), the left main bronchus (LMB), and the trachea (TRC). Five peripheral ARs were defined from each of the segmented lobes by excluding intra-parenchyma airway ARs (Fig. 1E).

Methods to transform the airway tree

Information from the two HRCT images was used to estimate the motion of the airway tree and its location within the PET imaging field.

Co-registering HRCT images. Though the subjects were imaged in a single session and were instructed to remain still on the table throughout the course of the study, in some cases motion between the two HRCT scans (taken between 30–60 min apart) was visually apparent. This motion is not related to breathing and needs to be isolated before a model of airway motion can be extracted from the images. To correct for differences in subject positioning, the upper spines in both images were segmented and co-registered using custom software (Matlab, Natick, MA). The co-registration algorithm sought to maximize overlap of the upper spines (using the Tanimoto Similarity Coefficient)[13] as the images were shifted relative to each other along the horizontal plane of the camera table without rotation (Fig. 1F); rotation was unnecessary since the narrowness of the gantry table prevents significant rotation.

Mapping TLC to MLV. The airways move and expand with lung inflation. Due to the fixed spatial resolution of HRCT, a greater extent of the airway tree can be reliably

FIG. 1. Panels illustrate the methods. **(A)** The TLC airway tree is trimmed to the sub-segmental generation to obtain a central airway tree ROI that is consistent across subjects. In *light blue* are umbrella-shaped cutting elements oriented with the segmental airways. In *green* are the trimmed portions of the tree. **(B)** The boundaries of the airways before and after the addition of sequential sources of blurring; the trimmed TLC @ MLV airway tree (*purple*), motion blur (*light purple*), PET blur (*orange*), including transformation and registration error (*darker yellow*), and the final PET mask discretized to the PET deposition image (*light yellow*). The boundaries represent the point where the voxel VI $>0.1\%$. **(C)** The nine airway tree ARs (shown in *saturated colors*), and iso-contours of their corresponding VIMs in matching colors representing 10%, 1%, and 0.1% VI are drawn for each AR (the color legend is shown in panel G). **(D)** Effect of mapping airway tree from TLC to MLV: Front and lateral projections of the airway tree (*Top*) rendered from a CT acquired at TLC (*red*) and one at MLV (*blue*); (*Bottom*) the same as above, but with the TLC tree mapped to the MLV. **(E)** A Rendering of the 14 Anatomical Regions (ARs). The color legend is shown in panel G. The lobar central airways are color matched to the lobes that they feed. The 16 cm PET field of view and the typical placement of the PET image are shown with the rectangle. The lung volume for this subject was 4.7 L at MLV (average volume at MLV was 3.2 L). **(F)** The co-registration of the TLC (*red*) and MLV (*blue*) spines. The *inset* shows the variability in the Tanimoto Similarity Coefficient of the upper spines as the images are shifted relative to each other. The *dark spot* shows that the HRCT images are best co-registered when the blue spine is shifted up and to the left. **(G)** A visualization of the VIMs. Each color indicates the VIM of a single AR. VIMs estimate of how homogenous activity within an AR appears in the radionuclear image. Where in a conventional black or while ROI each voxel is assigned to a specific AR, the rectangle shows how the voxel is influences by many ARs.

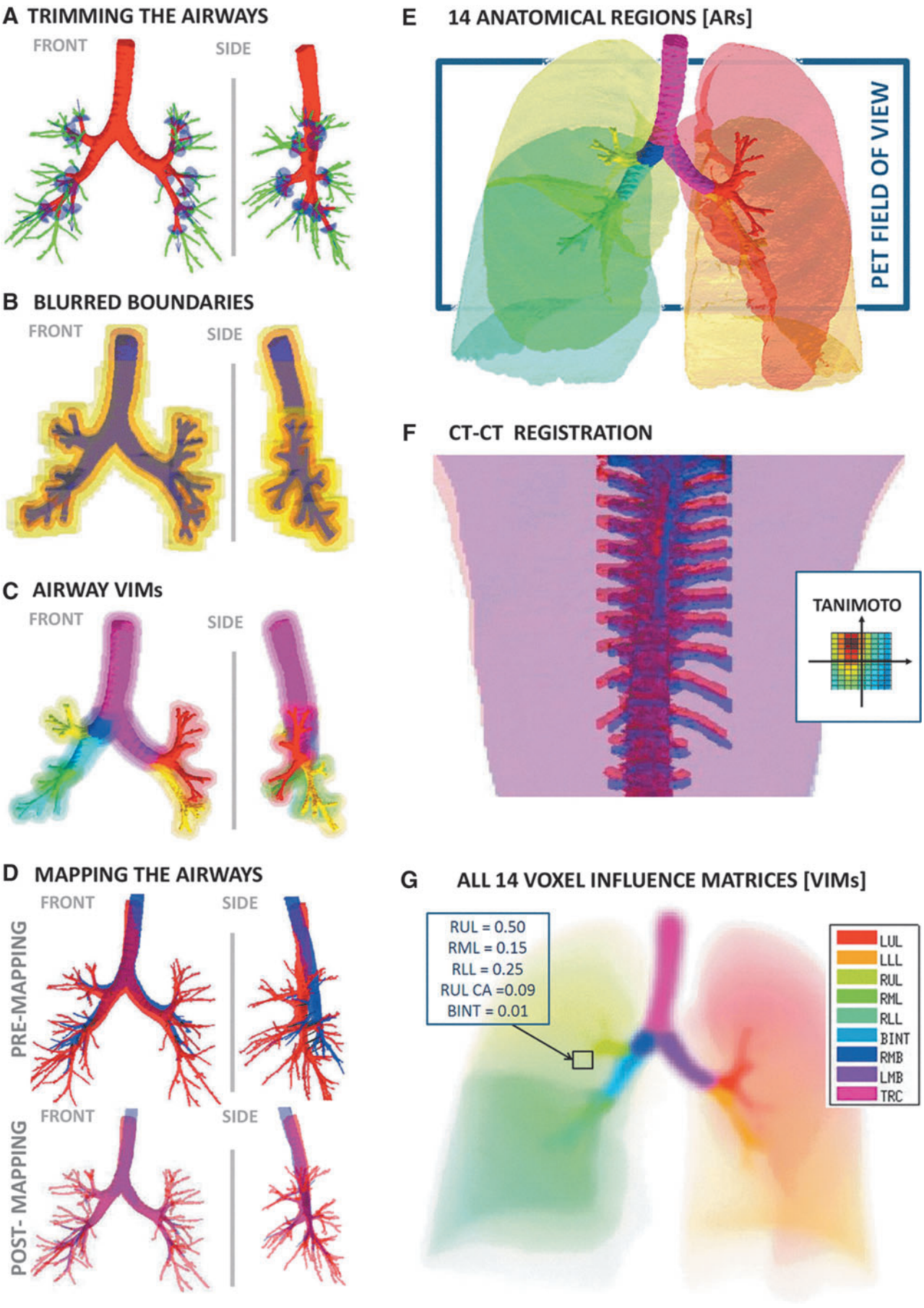
A TRIMMING THE AIRWAYS
FRONT
SIDE
B BLURRED BOUNDARIES
FRONT
SIDE
C AIRWAY VIMs
FRONT
SIDE
D MAPPING THE AIRWAYS
FRONT
SIDE
PRE-MAPPING
FRONT
SIDE
POST- MAPPING
E 14 ANATOMICAL REGIONS [ARs]
PET FIELD OF VIEW
F CT-CT REGISTRATION
TANIMOTO
G ALL 14 VOXEL INFLUENCE MATRICES [VIMs]
RUL = 0.50
RML = 0.15
RLL = 0.25
RUL CA =0.09
BINT = 0.01
LUL
LLL
RUL
RML
RLL
BINT
RMB
LMB
TRC

segmented from the TLC image compared with that from the MLV image. However, aerosol imaging with PET or SPECT is done during tidal breathing at a volume that varies around MLV. As a result, ROIs derived from the image at TLC cannot be directly used to analyze PET deposition images. To resolve this issue, the more detailed TLC airway tree was mapped to that at MLV by fitting an affine transformation to the positions of common anatomical bifurcations between the two scans. Mathematical details of this transformation are covered in Appendix I.

Co-registering the PET and HRCT Images. Even though in the PET–CT scanner PET and CT voxels are physically co-registered, in 12 of 14 subjects it was necessary shift the images relative to each other in order to overlay the deposition within the airway tree (visible as hot-spots in the PET image) with the airways rendered from the CT scan. In nine cases, shifting alone could not match the deposition pattern; the deposition image appeared to have been collected at a different average lung volume than that of MLV HRCT. In these cases a parametric function that allowed estimation of the airway position as a function of lung volume was used. The function was chosen so that the volume of the airways scaled linearly with lung volume, and is described in Appendix II. The parameterized transformation was used to identify the lung volume that resulted in the best visual overlay between PET and HRCT images. The simplest registration was employed when no evident improvement was gained by adding complexity to the co-registration (in order of preference: no added co-registration, shifting only co-registration, shifting plus volume co-registration).

Accounting for sources of blurring

This section introduces the use of Voxel Influence Matrices (VIMs) to model the sources of blurring and uncertainty in the PET images. Whereas the HRCT images are collected during a breath-hold, the PET or SPECT images are normally collected during breathing. Depending on the isotope and method, imaging times typically range from 10–60 minutes. The limited spatial resolutions of PET ($\sim$6 mm FWHM) and of SPECT ($\sim$15 mm FWHM) create partial volume and spill-over effects that further exaggerate the blurring. Blurring causes activity within an airway to be spread over a region that is significantly larger than the physical airway. When activity from a central airway, or peripheral region, does not include spill-over effects from other sources, the total activity from the region may be assessed by considering a large ROI that covers the entire blurred region.[3] However, when the counts from a region are affected by multiple sources (such as two neighboring airways), the activity within an enlarged ROI cannot be assigned to a single source. An additional blurring of the data comes from the discrete voxel representation of continuous data.

VIMs. Blurring, uncertainty, and discretization cause activity originating within an AR to be sampled in regions outside of it. Careful consideration of each of these effects permits the estimation of how activity within each AR contributes to activity within any voxel of the image. A VIM captures this measure for each AR. The sum of an AR's VIM is equal to its volume (in number of voxels); the VIM essentially redistributes the volume of the ARs to match their expected appearance in a PET image (Fig. 1C, 1G). VIMs are therefore a model of the apparent distribution of the AR volume as seen with PET divided by the voxel volume, and its units are this dimensionless fraction.

Modeling airway blur due to breathing motion. The PET image was taken during spontaneous tidal breathing that spanned a range of lung volumes around MLV. Using the parameterized transformation of the airway tree with lung volume, a model imitating airway motion during breathing was created. The function spreads the airway over the voxels through which airways moved during a tidal breath of 500 mL centered on the average lung volume during deposition imaging.

Limited PET resolution. The spatial resolution in PET (6 mm FWHM) is substantially lower than that of HRCT (0.3 mm). This leads to blurring by detecting activity originating within the central airways in voxels outside of the airways border. Thus, if ROIs were simply defined by following airway boundaries from HRCT, this would lead to substantial underestimation of the aerosol deposition within a given airway. A convolution with the point-spread function defined for the PET camera and reconstruction algorithm was utilized to further blur the motion-blurred ROI's.

Accounting for transformation and registration error. Even after co-registration, imperfections in the overlay between the CT airway mask and the high activity regions in the PET image were occasionally observed. These could arise from error in the TLC to MLV mapping (characterized by the root mean square error of the affine transformation (4 mm FWHM) or from limitations in the visual-guided registration described above (empirically estimated to be $\sim$5 mm FWHM). To account for these sources of uncertainty, the motion-blurred airway tree was further blurred by convolution with a single 3D Gaussian function that considered the effects of the PET point spread function, volume mapping, and co-registration error. The FWHM of this Gaussian function was defined as root sum of squares of the FWHM of each of the blurring effects (Fig. 1B).

Estimating airway and peripheral VIMs. To estimate airway VIMs, each of the nine airway ARs was blurred to model the effects of motion, PET resolution, and registration uncertainty (Fig. 1C). To estimate peripheral VIMs, each segmented lobe was first blurred for PET resolution and uncertainty and then the sum of all airway VIMs was removed from each element of the peripheral VIM (Fig. 1G).

Methods to evaluate deposition from the PET image

Two different methods to identify the aerosol distribution were implemented and applied to the same imaging data sets.

Black or white method. Here, the standard approach was used where ROIs were defined at PET resolution from their corresponding ARs segmented at CT resolution. Each voxel of the image was assigned to a single AR to avoid counting activity more than once. When a PET voxel included voxels from more than one AR, an algorithm was used to choose one of them. One algorithm considered for resolving this conflict was to assign PET voxels to the AR that has the

largest fraction of the voxel volume. However, this algorithm did not include voxels with smaller but still visible airways (that rarely occupy the majority of a voxel) into the airway ROIs. For this reason, the selection of ROI voxels was biased toward the airway ARs with a weighting factor of 100. Once the imaging field was divided into non-overlapping BW ROIs, the average specific activity (activity per unit volume) within each ROI was estimated by dividing the total activity sampled within the ROI by its volume.

Grayscale method. Here, a new approach was used where VIMs, and not ROIs, were defined for each of the ARs. As described above, VIMs simultaneously considered the influence of activity within all ARs on every voxel. In the contrast to the BW Approach, activity within any voxel could be contributed to multiple ARs. Thus, VIMs describe the effect of blurring, uncertainty, as well as the contribution of small airways (without the addition of an arbitrary factor to bias the small airways). Formally, considering m number of VIMs [R_i], of the same size as a PET deposition image [$_D$] we seek to estimate the average specific activity within each AR [x_i] that, after blurring, results in the best approximation of D, or:

$$\sum_{i=1}^{m} R_i x_i = D$$

This can be rewritten as a 2D linear algebra equation by reshaping the 3D VIMs and the deposition into 1D column vectors. Using Matlab notation (where R(:) is the column vector of any dimensional R):

$$\begin{bmatrix} | & | & & | \\ R_1(:) & R_2(:) & \dots & R_m(:) \\ | & | & & | \end{bmatrix} \begin{bmatrix} x_1 \\ x_2 \\ \vdots \\ x_m \end{bmatrix} = \Re X = D(:)$$

Nonphysical negative solutions of X were avoided using the Matlab's lsqnonneg ($\Re, D(:)$) function. Once X has been solved for, $\Re X$ is the deposition pattern based on average depositions within the ARs that is closest to D. This type of deposition pattern is also used for BW ROIs to generate the images in Figure 2A.

Comparison of the BW and grayscale approaches

To understand how the analysis method affected the quantification of the PET deposition images, they were applied to the same imaging data sets. Results from both methods where compared to each other and on how well they represented the PET images they were derived from.

Comparisons with the PET images. Analysis of the PET deposition images using either of the methods reduced imaging data from an average of 50,000 voxels to 14 degrees of freedom. Using these regional values and the 3D information from the ROIs or the VIMs, synthetic 3D images were created and compared to the original PET images. The goodness of fit was captured using the coefficient of determination [R^2] value. The R^2 was evaluated within the regions covered by BW ROIs excluding the large central airway ROIs to avoid the errors caused by activity in the esophagus, a region that was not accounted for in the ARs analysis. The statistical difference in R^2 between the two methods was evaluated using a paired t-test.

Inter-regional heterogeneity in aerosol deposition

For each AR, the values of aerosol deposition obtained with both methods were assessed for each in terms of the volume-normalized regional depositions (specific depositions). For BW method, regional specific deposition was estimated as the total activity within the ROI divided by the ROI volume. For the Grayscale method, the regional specific activity was the total activity assigned to the AR divided by the AR volume. The spatial heterogeneity of the distributions was characterized by a penetration index [PI] defined as the periphery-to-airway ratio of specific activities for each lobe. The variability of the PI values was characterized by the inter-subject variation in Lung Averages and by their inter-lobar COV (the standard deviation divided by the mean). The Lung Average was the average PI of the whole lung (without separating lobes) and its variability was characterized as the COV across subjects. The inter-lobar variability was the average of the COV of lobar values for each subject. The null hypothesis that all lobes behaved identically was tested using ANOVA with repeated measures. When differences were evident at the 5% alpha level, a Holm-Sidak test for multiple comparisons was used to test for individual differences between lobes.[14]

FIG. 2. Panels illustrate the results. **(A)** PET deposition images for three subjects (*first column*) contrasted with images of activity estimated with the two methods: BW and Grayscale. The estimated images are created by multiplying the ROIs used in each method by the estimated regional specific activities. The color scale within each row is kept constant with the *darkest red* corresponding to the point with highest activity. Both methods assume uniform deposition within the AR, which tends to diffuse hotspots in the estimated images. However, the Grayscale method tends to reproduce location and magnitude of hotspots better than the BW method. Note that the activity on the esophagus (present in the lower two PET images) is not represented in the projections since it was not defined as an AR (see discussion). **(B)** The coefficient of determination of the two methods. In all subjects the description of deposition with the Grayscale method is closer to the PET image ($p < 0.0001$) than with the BW method. **(C)** (*Left)* Projections of the ARs (at CT resolution) in *blue* overlaid with a projection of the deposition image (at PET resolution) in *red*. (*Right*) Projection of the estimated activity within the ARs (at CT resolution) using the Grayscale method. **(D)** The PI, TD, and ISC using Grayscale across lobes. Individual subject data are connected with *dashed lines*. The *solid line* is the average lobar values. No statistical difference was observed between a given lobe's TD. The LLL showed lower ISC than the lobes of the right lung (the strength of the line between the lobes under STATS indicates the strength of the P value).

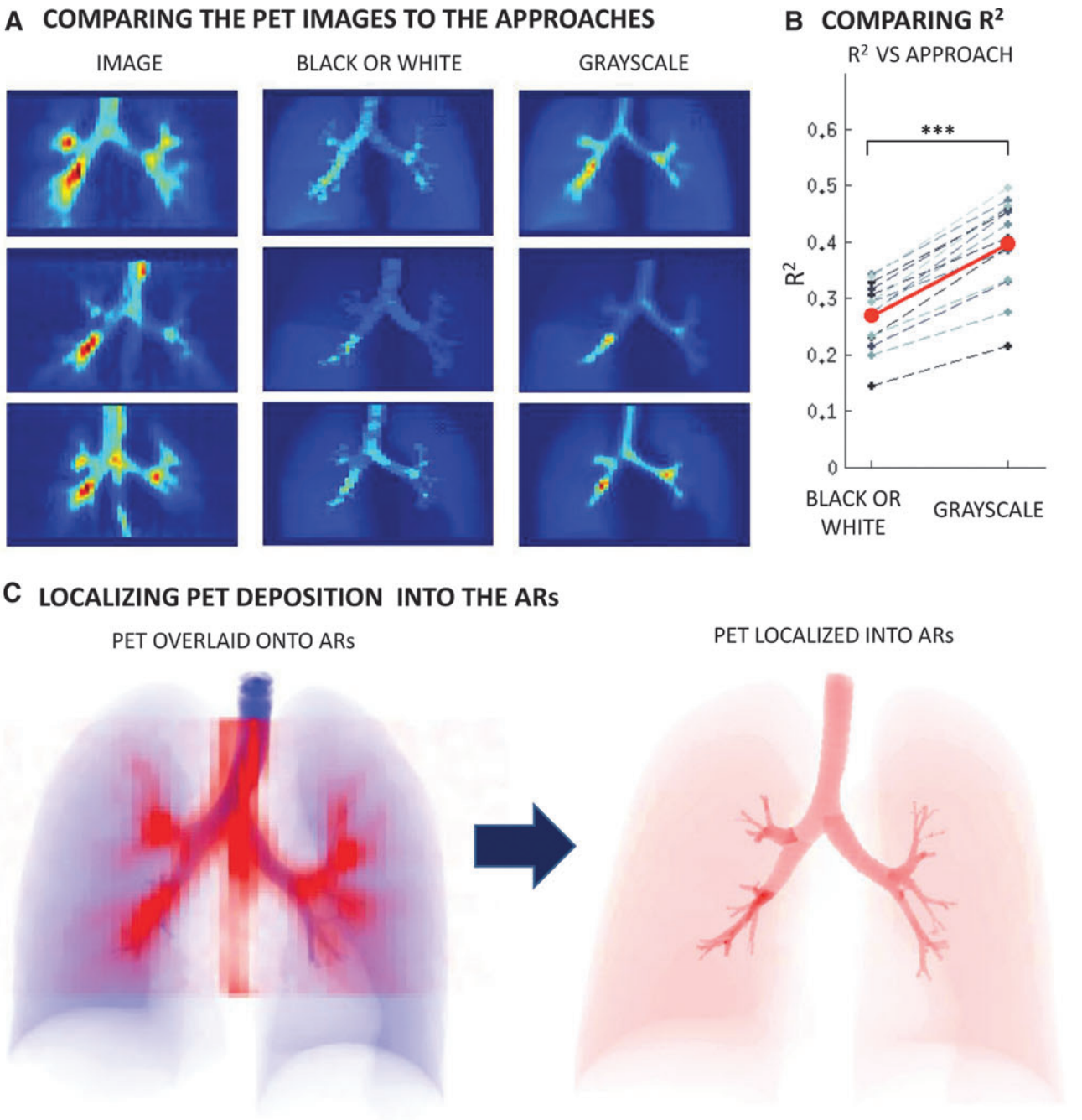
A COMPARING THE PET IMAGES TO THE APPROACHES
IMAGE
BLACK OR WHITE
GRAYSCALE
B COMPARING R²
R² VS APPROACH
***
R²
0.6
0.5
0.4
0.3
0.2
0.1
0
BLACK OR WHITE
GRAYSCALE
C LOCALIZING PET DEPOSITION INTO THE ARs
PET OVERLAID ONTO ARs
PET LOCALIZED INTO ARs
D LOBAR PI, TD, AND ISC
PENETRATION INDEX
PI [%]
NO STATISTICAL DIFFERENCE BETWEEN LOBES
LUL LLL RUL RML RLL
Lobe
TISSUE DOSING
TD [Total Lung Dose X 10⁻⁶/mg]
STATS
LUL
RLL
LLL
RML
RUL
INNER SURFACE CONCENTRATION
ISC [Total Lung Dose X 10⁻⁶/mm²]

Pharmacologically relevant units

From the data derived using the Grayscale method, the regional deposition could be described in terms of the Tissue Dosing (TD) and the Inner Surface Concentration (ISC). Evaluating this parameters required extraction of additional information from the HRCTs as follows.

Tissue dosing. In the peripheral ARs, TD was defined as the fraction of the total lung dose per unit of tissue mass. To exclude the volume occupied by blood, the regional ''tissue mass'' was estimated as the mass of water occupying half of the non-air volume if each lobar AR provided by the Apollo™ software.

Inner surface concentration. In airway ARs, ISC was defined to quantify the concentration of the aerosol per unit of airway surface. To calculate the ISC, it was necessary to estimate the surface area of each within each of the airway ARs using the method described in Appendix III.

Individual values of TD and ISC were characterized by the Lung Average and the Lobar COV, and differences between lobes were tested in the same manner as the PI.[14]

Results

Affine transformation

The affine transformation mapped the TLC airway tree to the MLV airway tree and reduced the average distance between locations of bifurcations by $92 \pm 4\%$ from 21.5 mm to 1.5 mm. The difference between the mapped bifurcations and the bifurcations locations at MLV had a FWHM of 4 mm. One example of this transformation is shown in Figure 1D.

Comparison of regional predictions

Anterior-posterior (A-P) projections of the deposition images of three of the subjects are compared with A-P projections of the synthetic images generated from the results for each of the two methods (Fig. 2A). Note that if the method captured all information from the original image, its synthetic image would be identical to the original PET image; discrepancies between the two indicate loss of information in the description of the data. The coefficient of determination of the Grayscale method was higher than the BW method for all subjects ($p < 0.0001$). This suggests that the Grayscale method is a better model to represent deposition observed in the PET image than with the BW method (Fig. 2B).

Penetration Index

The Grayscale method yielded lung average values of PI that were in average 7.0 ± 1.5 times those estimated using the BW method. At a lobar level, the factor ranged from 4 to more than 17 times. The relative variability in PI derived from the Grayscale method was higher among lobes and among subjects than the BW method (Table 1). Figure 2C shows how the Grayscale method uses VIMs to localize the blurred PET image in to the Anatomical Regions (ARs). The rest of the results presented below used the Grayscale method exclusively.

Table 1. The Lung Average and Lobar COV of the PI (Outer to Inner Specific Deposition Ratio), Presented for the Standard (BW) and Proposed Method (Grayscale)

Penetration Index (PI)	*Lung Average*	*Lobar COV*
Black or White	0.0565 ± 0.0161	0.21 ± 0.06
Grayscale	0.0086 ± 0.0039	0.30 ± 0.12

Lobar variability of specific deposition

There was high variability between in the total specific deposition among the lobes (Total Specific Deposition Lobar COV $= 0.33 \pm 0.12$). The variability was similar when the lobes were divided into central (Central Airways Specific Deposition Lobar COV $= 0.33 \pm 0.15$) and peripheral regions (Peripheral Specific Deposition Lobar COV $= 0.34 \pm 0.14$).

Heterogeneity of deposition in pharmacological terms

The Lung Average of Tissue Dosing (TD) was $2.11 \pm 0.40 \times 10^{-6}$ TLD/mg and the TD Lobar COV was 0.30 ± 0.14. No systematic difference was observed between TD of lobes. The Lung Average of Inner Surface Concentration (ISC) was $45 \pm 14 \times 10^{-6}$ TLD/mm^2, and the ISC Lobar COV was 0.31 ± 0.15. The LLL had a systematically lower ISC than the RUL ($p < 0.001$), the RLL ($p < 0.01$), and the RML ($p < 0.05$). The data are shown in Figure 2D.

Discussion

The methods above defined anatomically consistent regions of the lung (ARs) from HRCT. The concentration of aerosol deposited within the ARs were measured with lower resolution nuclear medicine imaging methods (PET and SPECT). A novel Grayscale method was developed to account for the effects of image blurring and uncertainty and for the contribution of airways too small to be identified with the limited resolution of the nuclear medicine imaging devices. In this method, Voxel Influence Matrices (VIMs) are used to evaluate the average specific deposition in each of the ARs and provide estimates of the pharmacologically relevant parameters TD and ISC.

The Grayscale method presented here is an extension of methods previously used to account for limited spatial resolution of imaging methods.[7–9] A similar formulation was described by Berker et al. to improve quantification of radionuclide therapy dosing,[7] based on the method introduced by Rousset et al.[8] to account for blurring in PET imaging of the brain. A version of Rousset's method was applied by Fleming et al.[9] to correct for partial volume effects between concentric shells in SPECT evaluation of aerosol deposition. Here, we generalized the concept by defining VIMs and adding breathing motion and co-registration uncertainty to the effect of limited imaging spatial resolution. Thus, VIMs can be thought as the influence (probability of effect * degree of effect) that activity within each AR has on measured activity at any point in the image. This represents a new method to analyze radionuclide images and shifts the paradigm from a Black-or-White to a more flexible Grayscale method.

Both methods were implemented and applied to the deposition on the lungs of bronchoconstricted asthmatics. In

these subjects, aerosol administration and imaging were performed in the supine position. While aerosol therapy is usually done in the upright position, having the actual airway geometry during deposition (which is different than upright) will allow to use this data for validating computational models of aerosol deposition.

Both the BW and Grayscale methods only explain part of the variance on the image (with R^2 of 0.27 and 0.39, respectively). A major source of the unexplained variance is the intra-AR variability; the method estimate the average deposition within each ARs, while in our data the deposition in the peripheral ARs was clearly concentrated near the visible large airways (see the first column in Fig. 2A). The averaging of activity within the AR diffuses the appearance of local hot spots. While we are interested in the average deposition within the ARs (and not in exactly reconstructing the PET images), the assumption of homogenous deposition within an AR affects the estimates of average specific deposition in the following ways: 1) It underestimates the spill-over of activity just beyond the central airway ARs, and thus overestimates the activity in the central airways; 2) The deposition in the portions of the lobes not included in the PET field of view (which are usually far from the central airways) was likely smaller than the average deposition in the measured part of the lobe; the assumption of homogeneous specific deposition throughout the lobe introduces error and tends to overestimate the amount of activity in the periphery. These issues might be mitigated by dividing the lung into a greater number of ARs. Despite this, Grayscale method yields a less diffuse description of deposition that is closer to the original PET image than the BW method ($p < 0.0001$).

To use the more detailed airway tree at TLC in the analysis, we formulated an affine transformation that described the displacement of bifurcation points between TLC and MLV (Appendix I). Parameterizing the affine by the global lung volume allowed estimation of blurring due to tidal breathing motion and also registration of the HRCT anatomy to the PET deposition images (Appendix II). Other methods have been used in the past to describe the displacement of landmarks between images (e.g., B-spline,[15,16] elastic-body spline,[17,18] thin-plate spline,[19,20] or moving least squares[21]). There are also alternative semi-automatic methods to extract the displacement of points in the lung,[21,22] as well as image registration techniques.[16,23] The simple affine transformation applied to automatically detected bifurcations was successful in mapping intrapulmonary airways from TLC to MLV (see Fig. 1D) and made it possible to parameterize the function in a way that linearly transformed the airway tree with global lung volume in a way consistent with the HRCT images. One of the alternative methods for modeling lung motion[16] assumes that each point of the tree moved along a line connecting the point in both images, where the position of point along the line was determined by the relative change in lung volume. If the motion of the airway tree did not include rotation, this method and the parameterized affine transformation would lead to similar results. Nonetheless, in the presence of the rotation expected by the inflation of a taper-shaped lung and chest wall (see Fig. 2D for an example), the inline motion method would not preserve the linear relationship between airway volume and lung volume.

The TLC image was taken before bronchoconstriction to maximize the fraction of the visible airway tree. While the position of the airways is not expected to be very different after bronchoconstriction, measurements of airway caliber taken from the TLC image likely do not reflect the bronchconstricted state.

Parameterizing the affine transformation by global lung volume is clearly an approximation. Relative expansion of the different lobes during breathing can be quite different from that of the total lung,[24] particularly in lungs with heterogeneous airway resistance as in asthmatic lungs during bronchoconstriction.[25] Even in normal lungs, changes of shape and volume depend on at least two independent parameters: the motion of both the diaphragm and that of the ribcage. In the absence of images, or models from which these parameters could be estimated, modeling the airway tree motion using a global lung volume parameter is a necessary simplification.

Even though in a PET-CT scanner the PET and CT images were acquired by the same instrument and their voxels were spatially co-registered, in a number of cases additional co-registration was required due to subject motion and/or differences in lung volume between the images. This co-registration was feasible because in our data, the central airways had substantially higher specific activity than the periphery. We believe that the highly central pattern of deposition observed likely resulted from the breathing pattern (spontaneous free tidal breathing), the bronchoconstricted state of the subject, and the aerosol specific to this study. In inhalation conditions with more peripheral deposition patterns, co-registration may be done with the external boundaries of the chest wall. It should be noted, however, that the PET to CT registration could erroneously mask two potential effects on the pattern of deposition: systematic sedimentation on the gravitationally-dependent side of the airway, and impaction along the inner walls distal to each bifurcation. However, even the complete sedimentation within an airway in the horizontal plane would only shift the deposition by one-half an airway diameter; registration based on the smaller of the central airways is only weakly sensitive to these differences. Similarly, the impaction effect would result in more distal deposition, but in a different direction for each bifurcation; global registration based on the whole tree should only be weakly sensitive to this effect as well. Reducing the time between scans and controlling the lung volume during both images should decrease the need for additional co-registration. Alternatively, co-registration techniques with fiducial markers visible in both imaging modalities (such as those in Berridge et al.[1]) could be used. Despite significant work automating the co-registration algorithm, in some cases visual identification of the best co-registration was ultimately necessary. Though this is common in deposition imaging,[3] it does reduce the reproducibility of the technique.

Our PET-CT imaging protocol used a HRCT image taken during breath hold at MLV to provide attenuation correction for PET images taken during breathing. While breathing over the course of the PET image, the anatomy is at a different position than in the HRCT image for most of the breathing cycle (below or above MLV). This leads to errors in the most peripheral regions of the lung, particularly close to the diaphragm and the ventral side of the lung where the largest distances of lung tissue movement occur during tidal breathing. Additionally, even though the CT attenuation scan at a volume equal to the average lung volume during

breathing, the filtered back projection reconstruction of the PET images can lead to negative values of activity near the chest wall. In our analysis, the negative values were set to zero to minimize the underestimation of activity in the periphery of the lung. The attenuation problems at the chest wall would be more exacerbated when the attenuation CT is acquired at FRC, as recommended by Dolovich and Bailey.[2] Errors due to attenuation correction can be improved using a conventional transmission scan or a long exposure low energy CT taken during breathing. Gating the images to the breathing cycle can also reduce these artifacts, though there is a necessary signal to noise penalty. Alternatively, breath holds at MLV (which are possible only with PET, such as those implemented by Lee[26]) after inhalation could yield sharper images with fewer co-registration and attenuation concerns. However, eliminating the blurring due to breathing would be at the expense of a reduction in signal to noise.

High activity was seen in the esophagus of many subjects, which resulted from swallowing activity that was deposited in the oral cavity. While Lee[26] manually separated the esophagus from the airways, we were unable to separate the two sources of activity confidently. Grayscale separation of these sources was hindered by the HRCT scans inability to delineate the location of the esophagus. In future studies, a rinse with water could be used after aerosol inhalation (if somewhat difficult in the supine position) to lower the activity in the esophagus.[7] Another limitation of the data is that the fraction of the trachea included in the PET and CT images varied between subjects. For these reasons, care must be taken interpreting values of deposition in the trachea, RMB and LMB.

The primary focus of this article is to describe an enhanced method to evaluate the anatomical distribution of an inhaled aerosol within the lungs using 3D imaging data from PET and HRCT. In future studies, the method could be used to estimate regional tissue dose and airway surface concentration as a percent of the inhaled dose. This will require assessment of radiation concentration in extra-pulmonary regions such as the oral cavity, pharynx, esophagus, and stomach that were not imaged in the current study.

To our knowledge, this is the first report of PET imaging data of asthmatics evaluating the centrality of the distribution pattern of an aerosol inhaled under our experimental conditions, namely: spontaneously breathing in the supine position and under provoked bronchoconstriction. It is of interest to note the exaggerated centralized pattern that is visually apparent from our data has a similar appearance to the deposition pattern of monodisperse 6 μm albuterol in aerosol observed with scintigraphy by Usmani et al.[28] in asthmatics in the sitting position. Given that those subjects were mild-to-moderate asthmatics with an $FEV_1 = 78\%$ predicted, and that the bronchodilator aerosol was inhaled in three consecutive breaths, it is unlikely that the bronchodilatory effect of albuterol had substantially reduced the degree of bronchoconstriction during the short inhalation period. In our study, the subjects had much higher baseline FEV_1 (102% predicted) but were challenged with methacholine at a dose to reduce FEV_1 by 20% at the beginning of the study, resulting therefore in equivalent degrees of obstruction during inhalation of the NH3-labeled aerosol.

We characterized the serial distribution of the aerosol deposition by the penetration index (PI) as recommended for standard for analysis of SPECT[3] and gamma camera deposition.[5] Here, the Grayscale method yielded average values of PI that were seven times lower than those obtained with the BW method. The main contributor to this difference is the different volumes over which the activity in the airways is concentrated; in the BW method the volume of the ROI is used (which is generally larger than the AR volume), while in the Grayscale method the actual AR volumes (built into the method) are used. This effect is largest in the central airways where the ROIs are 4.3 ± 1.5 times larger than the ARs. While it is possible to post process the BW deposition pattern to concentrate all the activity within the ROI into the AR volumes, this would neglect to account for activity that is in fact coming from the periphery. This problem becomes more significant with higher penetration indexes.

Average deposition on the three most central airway generations of each lobe (lobar, segmental, and sub-segmental) and on the rest of the lobe (periphery) were estimated in addition to the larger extra-pulmonary airways. The method could be extended to analyze individual segmental or even the sub-segmental airway ARs. However, as the images are divided into smaller regions approaching the length scale of blurring and uncertainty ($\sim$10 mm) Effects, it becomes increasingly difficult to separate the sources of the activity.

Aerosol deposition in 3D has also been analyzed using empirical models of airway tree morphometry to estimate deposition on different generations of the airway tree. In those methods the lung was divided into concentric shells (around the hilum[1,3,4,30] or the carina[2]). An estimate of the volume occupied by airways of each generation within each shell was derived from a symmetrical airway tree model,[4] or from a HRCT scan of a human lung cast.[30] Based on the assumption that activity within each generation is uniform throughout the lung, an estimate of the fraction of the deposition per generation was inferred.[3,4,30] Although the average deposition within each shell was assessed after correcting for partial volume effects, the effects of lung motion during breathing or co-registration uncertainty between the morphometric model and the anatomy were not considered. As *in vivo* imaging of aerosol deposition cannot presently visualize small airways, methods based on generalized morphometry seem the only viable method to estimate deposition within airways beyond the sub-segmental generations. However, our results showed that the deposition parameters in bronchoconstricted asthmatics were highly variable between lobes, and thus it would be at least necessary to analyze the lobes, or segments, separately before a shells approach could be meaningfully implemented. This approach could be integrated into the present method by defining generational ARs (at a lobar level) from generic morphometry or a lung cast. The resulting VIMs would avoid the loss of information that takes place when the airway generation is only described by its relative distance from the hilum.

The two pharmacologically relevant parameters, TD and ISC, were evaluated in the population. In the calculation of TD, the lobar deposition was assumed to be distributed over the tissue mass of the lobe. Tissue mass was estimated as one-half of the non-air fraction of the lung (provided by the Apollo software) to account for the volume occupied by blood. This assumption may be avoided by directly assessing regional blood volume using contrast media in CT or ^{11}CO in PET. Also, because the deposition in the periphery is not evenly distributed throughout the tissue (it is likely

concentrated in the airways), the TD presented here is only a first order approximation.

The inner lumen surface areas within the central airways were estimated to calculate regional ISC of the aerosol. It is important to note that the surface area measured from CT changes with lung volume. We chose to use the area measured at MLV because it provides a value that best approximates the inner area during breathing for that subject. The present measurement does not account for folding of the surface area that can happen in the smaller airways not visible with CT, and it is likely that the ISC is in fact lower than is estimated here in some airways.

The Grayscale method for analysis of regional aerosol deposition revealed additional heterogeneity between lobar deposition patterns in bronchoconstricted asthmatics. This average inter-lobar heterogeneity was similar whether the serial distribution was presented in terms of the volume normalized PI (Lobar COV = 0.30) or the parallel distribution expressed in pharmacologically relevant terms TD (Lobar COV = 0.30) and Lobar ISC (COV = 0.31). In practical terms, these results demonstrate that the serial (PI) or parallel (TD and ISC) heterogeneity may need to be taken into account when estimating the concentration of inhaled aerosol medications to heterogeneous lungs, If we consider the additional intra-lobar deposition heterogeneity not considered here, we venture to speculate that substantial parallel variability in tissue exposure within the lung could be responsible for significant reductions in effectiveness of certain inhaled medications.[6]

In summary, four main improvements of the proposed methodology over standard methods are presented here. First, anatomically consistent lobar airways are defined to allow unbiased comparisons between lobes and subjects. Second, subject movement, breathing motion, limited PET resolution, the contribution of small airways, and registration inaccuracies are accounted for in the estimation of regional anatomical deposition. Third, the more detailed airway tree imaged at TLC is used to interpret deposition imaged at lower lung volumes. Fourth, specific deposition values were correctly normalized by the airways true volume instead of the conventional ROI volume, thus avoiding gross underestimations of central airways specific activity. It was demonstrated that the standard Black or White ROI method substantially underestimated the specific deposition of aerosol in central airways. In contrast, the Grayscale method described the PET image more accurately, correctly assigning deposition to the volume of the AR, and yielded estimates of deposition terms such as tissue dose (TD) and inner surface concentration (ISC). These pharmacologically relevant terms could be important in translational research as well as in evaluation of novel aerosol delivery systems. More generally, the notion of voxel influence matrices, VIMs, represents a paradigm shift in the analysis of radiotracer localization within the anatomy that could have applications in other imaging modalities.

Acknowledgments

This work was sponsored by NIH grant HL68011, and by support from American Air Liquide Inc. Aerogen is thanked for providing the vibrating mesh nebulizers.

Author Disclosure Statement

This work was sponsored in part by American Air Liquide Inc. and Aerogen. However, there is no conflict of interest with these parties on any of the material presented in this publication.

References

1. Berridge MS, Lee Z, and Heald DL. Pulmonary distribution and kinetics of inhaled [11C]triamcinolone acetonide. J Nucl Med. 2000;41:1603–1611.
2. Dolovich MB, and Bailey DL. Positron emission tomography (PET) for assessing aerosol deposition of orally inhaled drug products. J Aerosol Med Pulm Drug Deliv. 2012;25:52–71.
3. Fleming J, Bailey DL, Chan HK, Conway J, Kuehl PJ, Laube BL, and Newman S. Standardization of techniques for using single-photon emission computed tomography (SPECT) for aerosol deposition assessment of orally inhaled products. J Aerosol Med Pulm Drug Deliv. 2012;25:29–51.
4. Fleming J, Nassim M, Hashish A, Bailey A, Conway J, Holgate S, Halson P, Moore E, and Martonen T. Description of pulmonary deposition of radiolabeled aerosol by airway generation using a conceptual three dimensional model of lung morphology. J Aerosol Med. 1995;8:341–356.
5. Newman S, Bennett WD, Biddiscombe M, Devadason SG, Dolovich MB, Fleming J, Haeussermann S, Kietzig C, Kuehl PJ, Laube BL, Sommerer K, Taylor G, Usmani OS, and Zeman KL. Standardization of techniques for using planar (2D) imaging for aerosol deposition assessment of orally inhaled products. J Aerosol Med Pulm Drug Deliv. 2012;25:S10–28.
6. Venegas J, Winkler T, and Harris RS. Lung physiology and aerosol deposition imaged with positron emission tomography. J Aerosol Med Pulm Drug Deliv. 2013;26:1–8.
7. Berker Y, Goedicke A, Kemerink GJ, Aach T, and Schweizer B. Activity quantification combining conjugate-view planar scintigraphies and SPECT/CT data for patient-specific 3-D dosimetry in radionuclide therapy. Eur J Nuclear Med Mol Imaging. 2011;38:2173–2185.
8. Rousset OG, Ma Y, and Evans AC. Correction for partial volume effects in PET: Principle and validation. J Nuclear Med. 1998;39:904–911.
9. Fleming JS, Sauret V, Conway JH, Holgate ST, Bailey AG, and Martonen TB. Evaluation of the accuracy and precision of lung aerosol deposition measurements from single-photon emission computed tomography using simulation. J Aerosol Med. 2000;13:187–198.
10. Asthma GIf. *Global Strategy for Asthma Management and Prevention.* NIH Publication. 2002.
11. Finlay P, Martin A, Katz I, Vecellio L, Caillibotte G, and Venegas J. Aerosol delivery from a vibrating mesh nebulizer with holding chamber in helium/oxygen versus air. J Aerosol Med Pulm Drug Deliv. 2013;26:A20.
12. Finlay WH. *The Mechanics of Inhaled Pharmaceutical Aerosols: An Introduction.* Academic Press, 2001.
13. Lipkus AH. A proof of the triangle inequality for the Tanimoto distance. J Math Chem. 1999;26:263–265.
14. G C. Anovarep: Compute the Anova for repeated measures and Holm-Sidak test for multiple comparisons if Anova is positive. 2008.
15. Lee S, Wolberg G, Chwa KY, and Shin SY. Image metamorphosis with scattered feature constraints. Visual Computer Graphics, IEEE Trans. 1996;2:337–354.
16. Yin Y, Hoffman EA, Ding K, Reinhardt JM, and Lin CL. A cubic B-spline-based hybrid registration of lung CT images for a dynamic airway geometric model with large deformation. Phys Med Biol. 2010;56:203.

17. Davis MH, Khotanzad A, Flamig DP, and Harms SE. Elastic body Splines: A physics based approach to coordinate transformation in medical image matching. Computer-Based Medical Systems, 1995., Proc Eighth IEEE Symp. IEEE; 1995; pp. 81–88.
18. Wörz S, and Rohr K. Physics-based elastic registration using non-radial basis functions and including landmark localization uncertainties. Computer Vision Image Understand. 2008;111:263–274.
19. Rohr K, Stiehl HS, Sprengel R, Buzug TM, Weese J, and Kuhn M. Landmark-based elastic registration using approximating thin-plate splines. Medical Imaging, IEEE Trans. 2001;20:526–534.
20. Johnson HJ, and Christensen GE. Consistent landmark and intensity-based image registration. Medical Imaging, IEEE Trans. 2002;21:450–461.
21. Castillo R, Castillo E, Guerra R, Johnson VE, McPhail T, Garg AK, and Guerrero T. A framework for evaluation of deformable image registration spatial accuracy using large landmark point sets. Phys Med Biol. 2009;54:1849.
22. Murphy K, van Ginneken B, Pluim J, Klein S, and Staring M. Semi-automatic reference standard construction for quantitative evaluation of lung CT registration. Medical Image Comput Computer-Assist Intervent 2008. 2008:1006–1013.
23. Ding K, Bayouth JE, Buatti JM, Christensen GE, and Reinhardt JM. 4DCT-based measurement of changes in pulmonary function following a course of radiation therapy. Med Phys. 2010;37:1261.
24. Milic-Emili J, Henderson J, Dolovich M, Trop D, and Kaneko K. Regional distribution of inspired gas in the lung. J Appl Physiol. 1966;21:749–759.
25. Venegas J. Linking ventilation heterogeneity and airway hyperresponsiveness in asthma. Thorax. 2007;62:653–654.
26. Lee Z, and Berridge MS. PET imaging-based evaluation of aerosol drugs and their delivery devices: Nasal and pulmonary studies. Medical Imaging, IEEE Trans. 2002;21:1324–1331.
27. Sturm R. Modeling the deposition of bioaerosols with variable size and shape in the human respiratory tract–-A review. J Adv Res. 2012;3:295–304.
28. Usmani OS, Biddiscombe MF, and Barnes PJ. Regional lung deposition and bronchodilator response as a function of β2-agonist particle size. Am J Respir Crit Care Med. 2005;172:1497–1504.
29. Fleming JS, Epps BP, Conway JH, and Martonen TB. Comparison of SPECT aerosol deposition data with a human respiratory tract model. J Aerosol Med. 2006;19:268–278.
30. Fleming JS, Sauret V, Conway JH, and Martonen TB. Validation of the conceptual anatomical model of the lung airway. J Aerosol Med. 2004;17:260–269.

Received on December 16, 2013
in final form, June 3, 2014

Reviewed by:
Joy Conway
Myrna Dolovich
Marc Berridge

Address correspondence to:
Jose Venegas, PhD
Massachusetts General Hospital, Edwards 410A
55 Fruit St.
Boston, MA 02114

E-mail: jvenegas@alum.mit.edu

(Appendix follows →)

Appendix I

Affine transformation

An affine transformation is any transformation under which a straight line in the original space remains a line in the transformed space. In 3D this allows for any combination of translation, scaling, and rotation. If a series of points that are positioned at points in the TLC image move to positions in the MLV image, we can organize the points into corresponding rows of matrices X_{TLC} and X_{MLV} then add a column of ones to the end of each matrix. We can write the system of equations for the affine transformation matrix B_{TLC}^{MLV} (which can be solved using least squares with the backslash operator in Matlab):

$$B_{TLC}^{MLV} {X_{TLC}}^T = {X_{MLV}}^T,$$

$$\text{or } B_{TLC}^{MLV} = [X_{TLC} \backslash X_{MLV}]^T = \begin{bmatrix} R_{TLC}^{MLV} & & & d_{TLC}^{MLV} \\ 0 & 0 & 0 & 1 \end{bmatrix}$$

By applying all points in the TLC airway tree to the B_{TLC}^{MLV} affine we were able to transform the TLC airways to MLV.

Appendix II

Volume-corrected affine parameterization

The above affine transformation yields a transformation for point in the TLC image to points in the MLV image. We sought to parameterize this transformation with lung volume to find the transformation from TLC to other lung volumes (identified with subscript VOL). As the affine transformation from TLC to TLC is the identity matrix, one simple way is to do this is to suggest that each of the components of the affine moves from its value in the identity matrix at TLC to corresponding B_{TLC}^{MLV} entry at MLV with a single volume dependent parameter s_{VOL}:

$$\hat{B}_{TLC}^{VOL} = s_{VOL}\left(B_{TLC}^{MLV} - I\right) + I = \begin{bmatrix} & \hat{R}_{TLC}^{VOL} & & d_{TLC}^{VOL} \\ 0 & 0 & 0 & 1 \end{bmatrix},$$

$$\text{where } s_{VOL} = \frac{(V_{VOL})^{\frac{1}{3}} - (V_{TLC})^{\frac{1}{3}}}{(V_{MLV})^{\frac{1}{3}} - (V_{TLC})^{\frac{1}{3}}}$$

However, this does not ensure that the actual airways volume under the transformation will match the expected airways size at V_{VOL}. It can be shown that the absolute value of the determinant of R (the upper three by three of any affine matrix B (which holds a combination of the rotation and scaling effects) is equal to the net volume scaling of B. A correction factor was applied to R to scale the airways to their expected volume for a given lung volume. The expected positive scaling factor k_{VOL} at a given V_{VOL} is:

$$k_{VOL} = \left(\frac{V_{VOL} - V_{TLC}}{V_{MLV} - V_{TLC}}\right)\left(\left|\det\left(R_{TLC}^{MLV}\right)\right| - 1\right) + 1$$

Multiplying a 3×3 matrix with a constant C results in an amplification of the determinant by C^3. The correct scaling C to yield a volume scaling of k_{VOL} is:

$$C = \left(\frac{k_{VOL}}{\left|\det\left(\hat{R}_{TLC}^{VOL}\right)\right|}\right)^{\frac{1}{3}}$$

The scaling is done about the origin of the coordinate system and can cause the airways to change position. To counter this effect, we add a displacement to the corrected affine that ensures that the corina (situated at TLC at point x_{corina}) does not move as a consequence of the scaling. One possible volume corrected affine parameterization is then:

$$B_{TLC}^{VOL} = \begin{bmatrix} & C\hat{R}_{TLC}^{VOL} & & \left((1-C)\hat{R}_{TLC}^{VOL} x_{corina} + d_{TLC}^{VOL}\right) \\ 0 & 0 & 0 & 1 \end{bmatrix}$$

Note that this gives the desired scaling k_{VOL} at all positive lung volumes:

$$\begin{aligned} \left|\det\left(B_{TLC}^{VOL}\right)\right| &= \left|\det\left(C^{\frac{1}{3}}\hat{R}_{TLC}^{VOL}\right)\right| \\ &= \left|\left(\left(\frac{k_{VOL}}{\left|\det\left(\hat{R}_{TLC}^{VOL}\right)\right|}\right)^{\frac{1}{3}}\right)^3 \det\left(\hat{R}_{TLC}^{VOL}\right)\right| \\ &= |k_{VOL}| = k_{VOL}\big|_{(k_{VOL} \geq 0)} \end{aligned}$$

The carina position also does not shift under the correction:

$$\begin{aligned} & B_{TLC}^{VOL}\begin{bmatrix} x_{corina} \\ 1 \end{bmatrix} \\ &= \begin{bmatrix} & C\hat{R}_{TLC}^{VOL} & & \left((1-C)\hat{R}_{TLC}^{VOL} x_{corina} + d_{TLC}^{VOL}\right) \\ 0 & 0 & 0 & 1 \end{bmatrix}\begin{bmatrix} x_{corina} \\ 1 \end{bmatrix} \\ &= \begin{bmatrix} \left(C\hat{R}_{TLC}^{VOL} x_{corina} + (1-C)\hat{R}_{TLC}^{VOL} x_{corina} + d_{TLC}^{VOL}\right) \\ 1 \end{bmatrix} \\ &= \begin{bmatrix} & \hat{R}_{TLC}^{VOL} & & d_{TLC}^{VOL} \\ 0 & 0 & 0 & 1 \end{bmatrix}\begin{bmatrix} x_{corina} \\ 1 \end{bmatrix} = \hat{B}_{TLC}^{VOL}\begin{bmatrix} x_{corina} \\ 1 \end{bmatrix} \end{aligned}$$

Appendix III

Airway surface area and volume

The volume of the intrapulmonary central airways at TLC was found by counting the number of voxels within the airways. The surface area of the airways was estimated using the Apollo measurements of the lobar and segmental airways. Measurements of the diameter and length of the sub-segmental airways could not be made reliably and these airways are not included in the surface measurement. The determinant of the affine operator gives the ratio of the airways' volume after transformation to that before transformation. We used this to scale the TLC airway volume to MLV. Similarly we used this factor raised to the 2/3 to scale the TLC airway area to MLV.

Abbreviations Used

AR = An **A**natomical **R**egion is the physical volume of interest independently of how it shows up in any of the imaging modalities.
BINT = **B**ronchus **Int**ermedius AR.
BW = **B**lack or **W**hite method for interpreting regional information in image using binary ROIs.
COV = The **C**oefficient **O**f **V**ariation is the standard deviation normalized by the mean of a distribution.
D: = The aerosol deposition image with units of specific deposition.
FEV_1: = The Forced Expiratory Volume in 1 second for a given subject in an effort from TLC.
FWHM = **F**ull **W**idth **H**alf **M**aximum of a distribution is a measure of a distribution. For a Gaussian distribution, FWHM is 2.4 times the standard deviation.
Grayscale = A method of interpreting regional information in an image using VIMs with values that range from zero to one.
HRCT, CT = **H**igh **R**esolution **C**omputed **T**omography images use X-rays to create clear pictures of the anatomy with a typical resolution of 0.3mm.
ISC = The **I**nner **S**urface **C**oncentration is the dose delivered to an airway per unit surface area.
LUL, LLL, RUL, RML, RLL = **L**eft **U**pper **L**obe, **L**eft **L**ower **L**obe, **R**ight **U**pper **L**obe, **R**ight **M**iddle **L**obe, and **R**ight **L**ower **L**obe, respectively.
LUL CA, LLL CA, RUL CA, RML CA, RLL CA = The **C**entral **A**irways of each lobe defined as the lobar through subsegmental airways.
MLV = **M**ean **L**ung **V**olume is the average volume during tidal breathing.
MMAD = **M**ass **M**edian **A**erodynamic **D**iameter is a measure of the median aerosol diameter.
^{13}N-NH3 = Ammonia labeled with radioactive nitrogen with a half-life of 10 minutes used in this study to follow nebulized aerosols.
PC_{20} = The dose of Methacholine that results in a 20% reduction in FEV_1 in a given subject.
PI = The **P**enetration **I**ndex is the periphery-to-airway ratio of specific deposition.
PET = **P**ositron **E**mission **T**omography follows radiolabeled tracers in the body with a typical resolution of 6.0mm.
PET-CT, SPECT-CT = Imaging device that can sequentially take both HRCT and PET or SPECT images without repositioning the subject on the gantry.
ROI = A **R**egion **O**f **I**nterest is a subset of voxels within an image that cover an AR used in Black or White analysis of radiolabeled images.
RMB, LMB = **R**ight and **L**eft **M**ain **B**ronchus ARs.
Specific Deposition = The deposition within a region normalized by its volume.
R_i,$\mathfrak{R}$ = The ith AR's three dimensional VIM, and a 2D matrix with all VIMs arranged in column vectors;
SPECT = **S**ingle-**P**hoton **E**mission **C**omputed **T**omography follows radiolabeled tracers within the body with a typical resolution of 15mm.
TD = The **T**issue **D**osing is the dose delivered to a region normalized by the local tissue volume.
TLC = Total Lung Capacity is the maximal volume of the lung.
TLD = The **T**otal **L**ung **D**ose is the cumulative deposition in all lobes and lobar central airways.
TRC = The **Trac**hea AR.
VIM = A **V**oxel **I**nfluence **M**atrix considers how average activity within each AR influences the measured activity within each voxel in a radiolabeled image. VIMs are used in the Grayscale approach.
VMD = **V**olume **M**edian **D**iameter.
GSD = **G**eometric **S**tandard **D**eviation.
X = A vector of each AR's specific deposition.